Supporting Information for

Formation of Stanley Patch volcanic cone:

New insights into the Evolution of Deception Island Caldera (Antarctica)

J. Hopfenblatt [1,2], A. Geyer [1], M. Aulinas [2], A.M. Álvarez-Valero [3], G. Gisbert [4], G. Kereszturi [5], G. Ercilla [6], M. Gómez-Ballesteros [7], A. Márquez [8], D. García-Castellanos [1], D. Pedrazzi [1], H. Sumino [9], A. Höskuldsson [10], S. Giralt [1], C. Angulo-Preckler [11,12]

1. Geosciences Barcelona, Geo3Bcn, CSIC, Lluis Sole i Sabaris s/n, 08028 Barcelona, Spain

2. Departament de Mineralogia, Petrologia i Geologia Aplicada. Universitat de Barcelona, Marti Franques s/n, 08028 Barcelona, Spain

3. Departamento de Geología, Universidad de Salamanca, 37008 Salamanca, Spain

4. Instituto de Geociencias, CSIC-UCM, Severo Ochoa 7, 28040 Madrid, Spain

5. Volcanic Risk Solutions, School of Agriculture and Environment, Massey University, Palmerston North, New Zealand

6. Instituto de Ciencias del Mar, ICM-CSIC. Continental Margin Group. Paseo Marítimo de la Barceloneta, 37-49; 08003 Barcelona, Spain

7. Instituto Español de Oceanografía, C/Corazón de María 8, 28002 Madrid, Spain

8. Área de Geología, ESCET, Universidad Rey Juan Carlos, 28933 Móstoles, Madrid, Spain

9. Department of General Systems Studies, Graduate School of Arts and Sciences, University of Tokyo, Japan

10. Nordic Volcanological Center, Institute of Earth Sciences, University of Iceland, Sturlugata 7, 101 Reykjavik Iceland

11. Norwegian College of Fishery Science. UiT The Arctic University of Norway, Tromsø, Norway

12. IRBio (Research Institute of Biodiversity), Barcelona, Spain

Contents of this file

Figures S1 to S13
Table S1

Introduction

This document contains the supporting information and figures regarding the:

(a) Volcanic rock samples collected at the shallowest sector of the crater rim of Stanley Patch submerged volcano (Deception Island, Antarctica)
(b) Geophysical study carried out during the 2017/2018 Spanish Antarctic Campaign and the Antarctic GALILEO-IHM cruise aboard the R/V Hespérides (2017 / 2018)
(c) Geomorphometry analysis carried out at Stanley Patch volcano
(d) Results of the outburst flood model simulations.

A detailed description about when and how the data were collected or created and the processing steps used is provided in the main text.

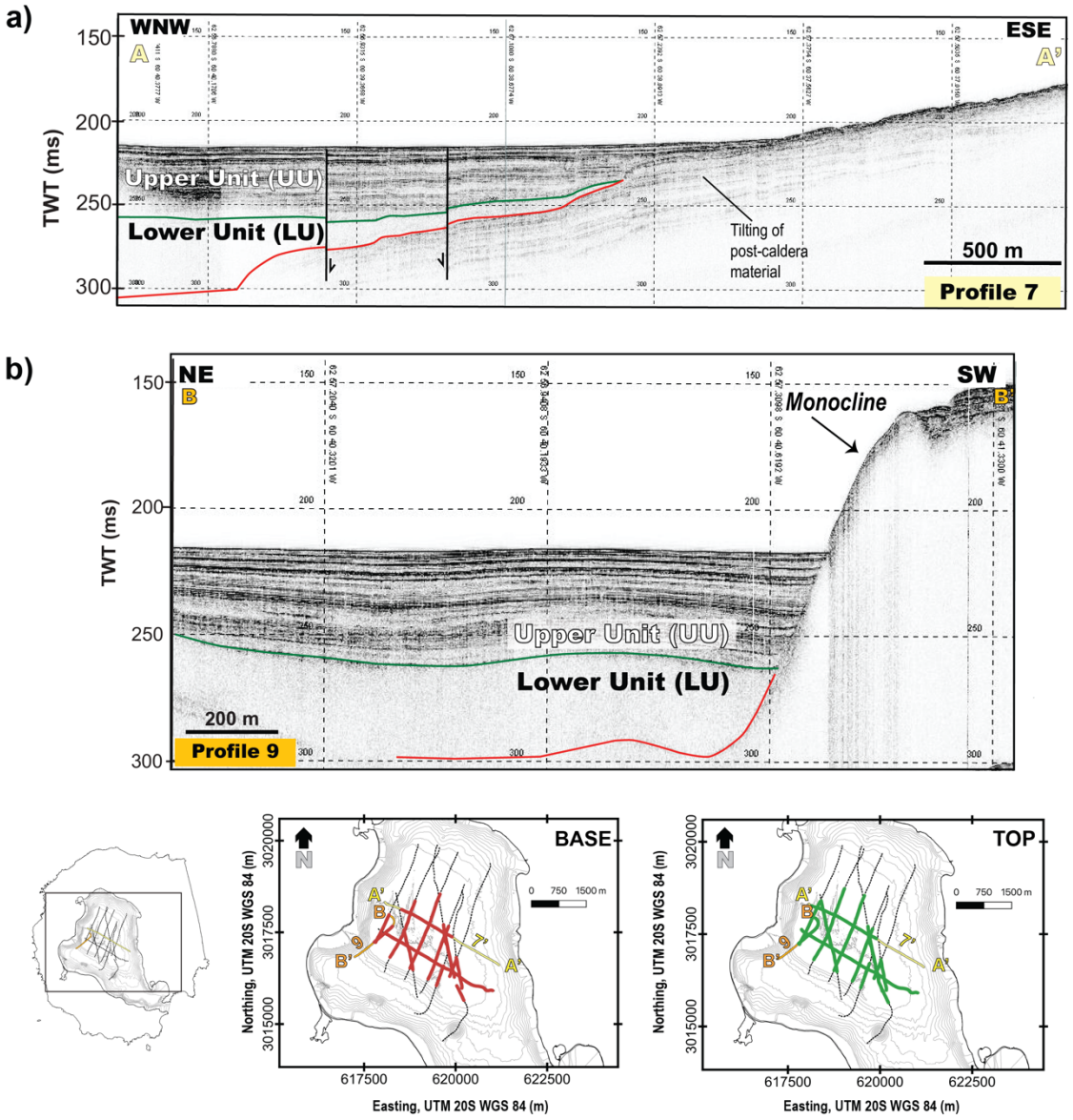

Figure S1. (a) to (g) seismic profiles obtained within Port Foster. The top and base of the Lower Unit are highlighted in green and red, respectively. The location of the profiles is shown in the inset (bottom left) and maps (bottom center and right). The red and green colored thick lines in the maps indicate the lateral coverage where the base (red) and top (green) of the Lower Unit are observable in the different seismic profiles. Seismic profiles have been analyzed with the Kingdom Suite (Version 8.4) software. The seismic profiles are available at SEANOE repository: https://doi.org/10.17882/77208.

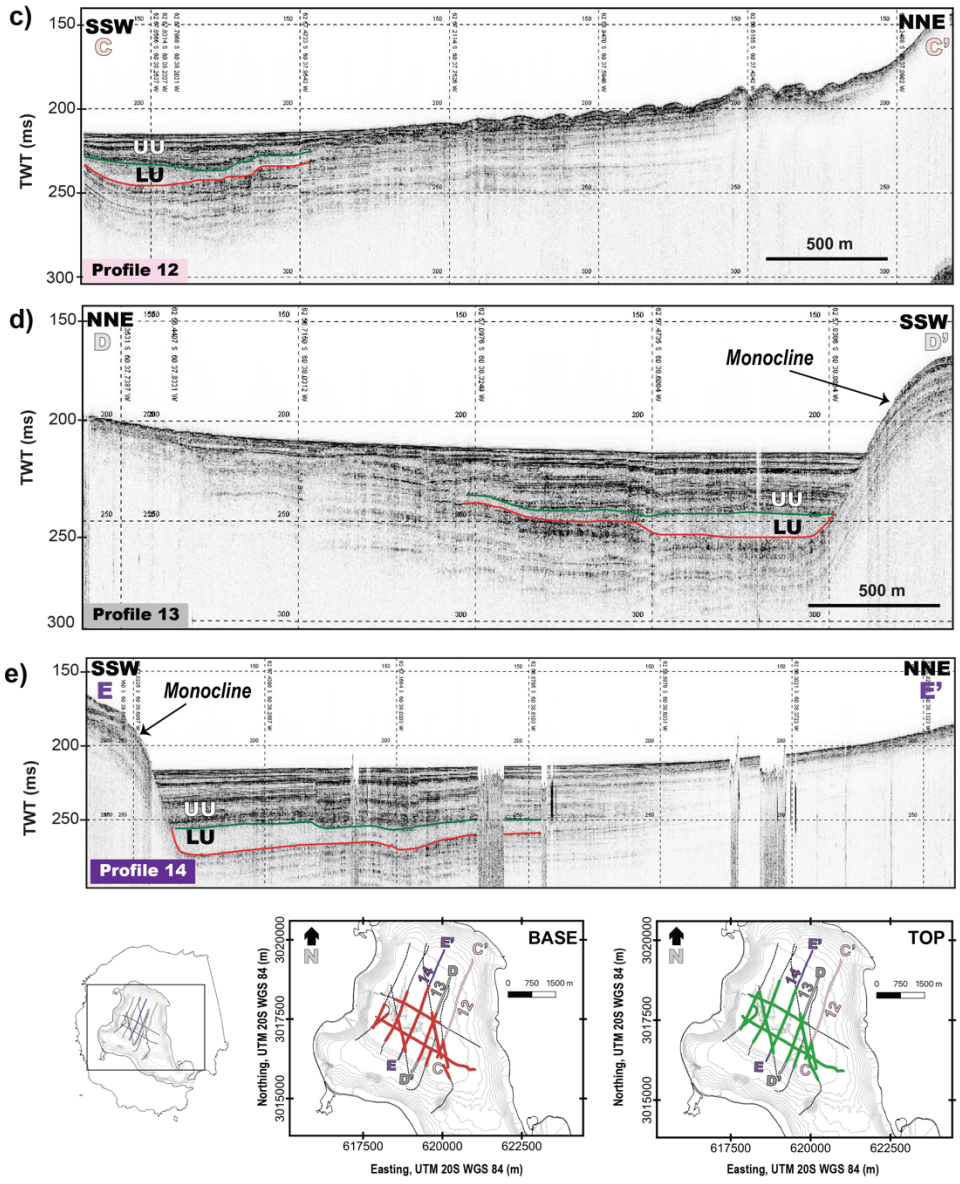

Figure S1. Continuation.

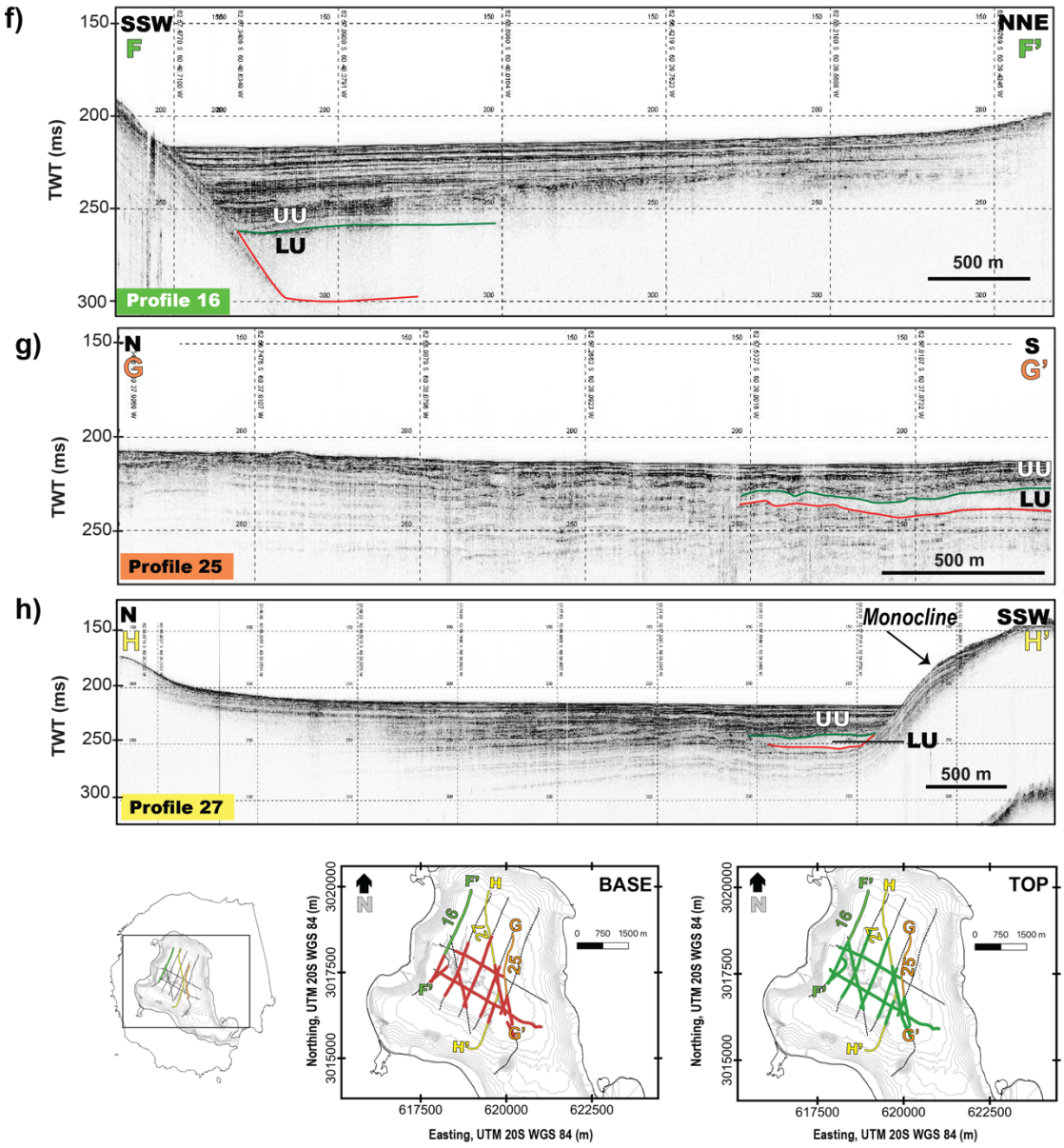

Figure S1. Continuation.

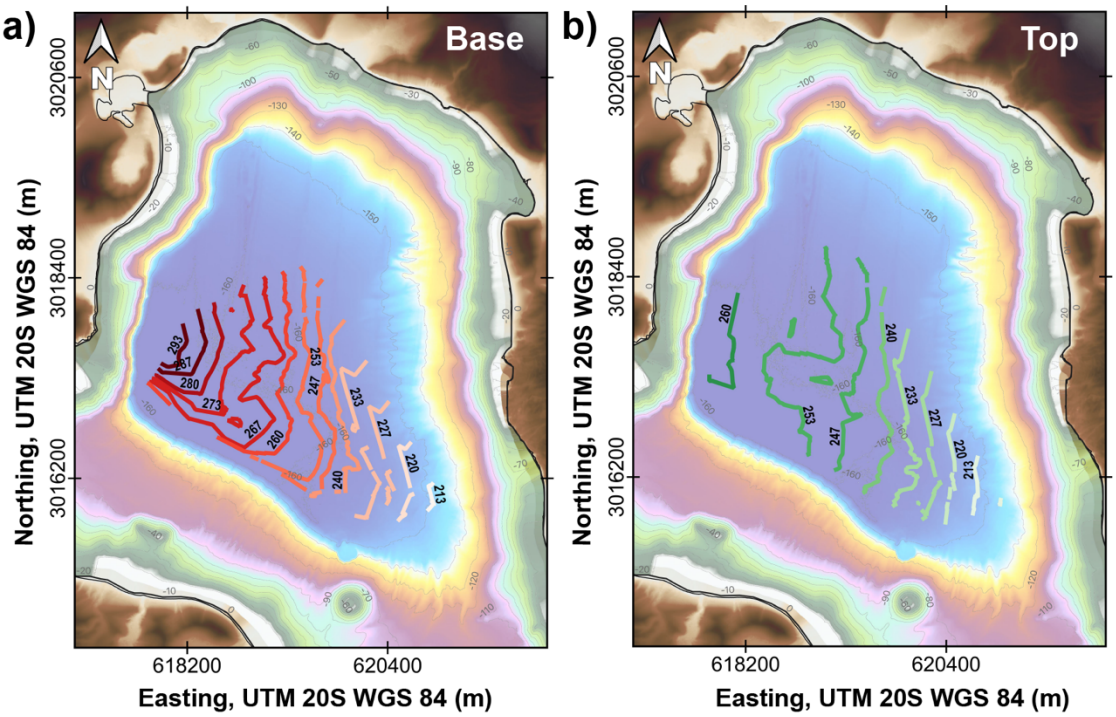

Figure S2. Digital Elevation Model of Port Foster including the isobaths (in ms) for the base (a) and top (b) of the acoustically semi-transparent Lower Unit (LU) described in the text and highlighted in the seismic profiles of Figure 6 and S1. See main text for further details.

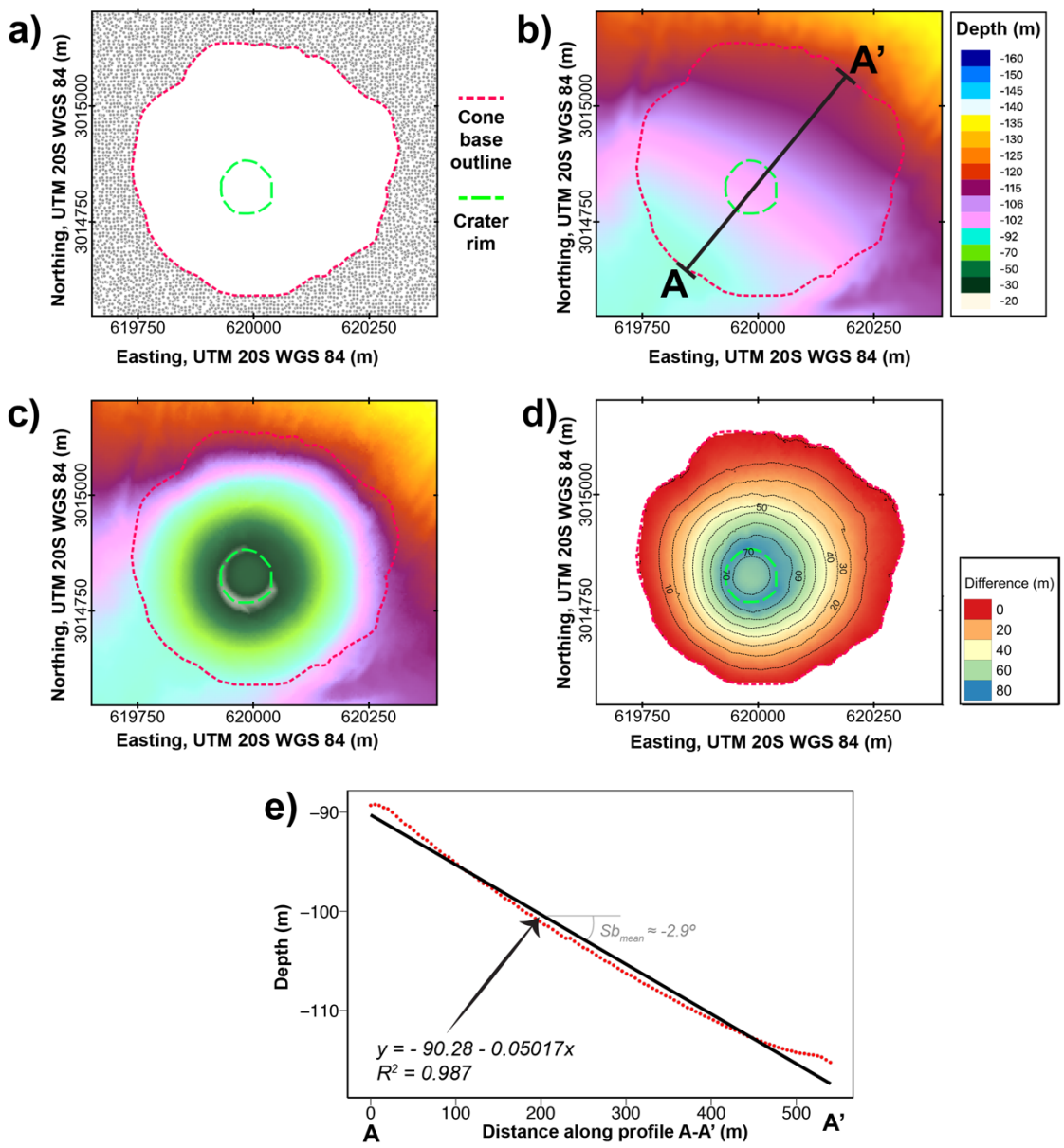

Figure S3. (a) Shapefile map of the elevation data points around Stanley Patch volcano used to interpolate the pre-eruptive basal surface. The cone base outline and the crater rim are also indicated. (b) Pre-eruptive basal surface interpolated from the elevation data points shown in a) and by applying the *v.surf.bspline* function of GRASS GIS software version 7.6 (available at: http://grass.osgeo.org), which performs a bilinear/bicubic spline interpolation with Tykhonov regularization. c) 4 × 4 m grid size Digital Elevation Model (DEM) of Stanley Patch volcano developed by means of the open source QGIS software version 3.10 "A Coruña" (available at: http://www.qgis.org/). Legend as per b). d) Cone height above the pre-eruptive basal level at each pixel obtained by difference from b) and c). e) Elevation points obtained along a A-A' profile (see b)) aligned along the maximum dip direction of the basal surface. The average slope of the basal plane (Sb_{mean}) is then obtained by applying a linear regression.

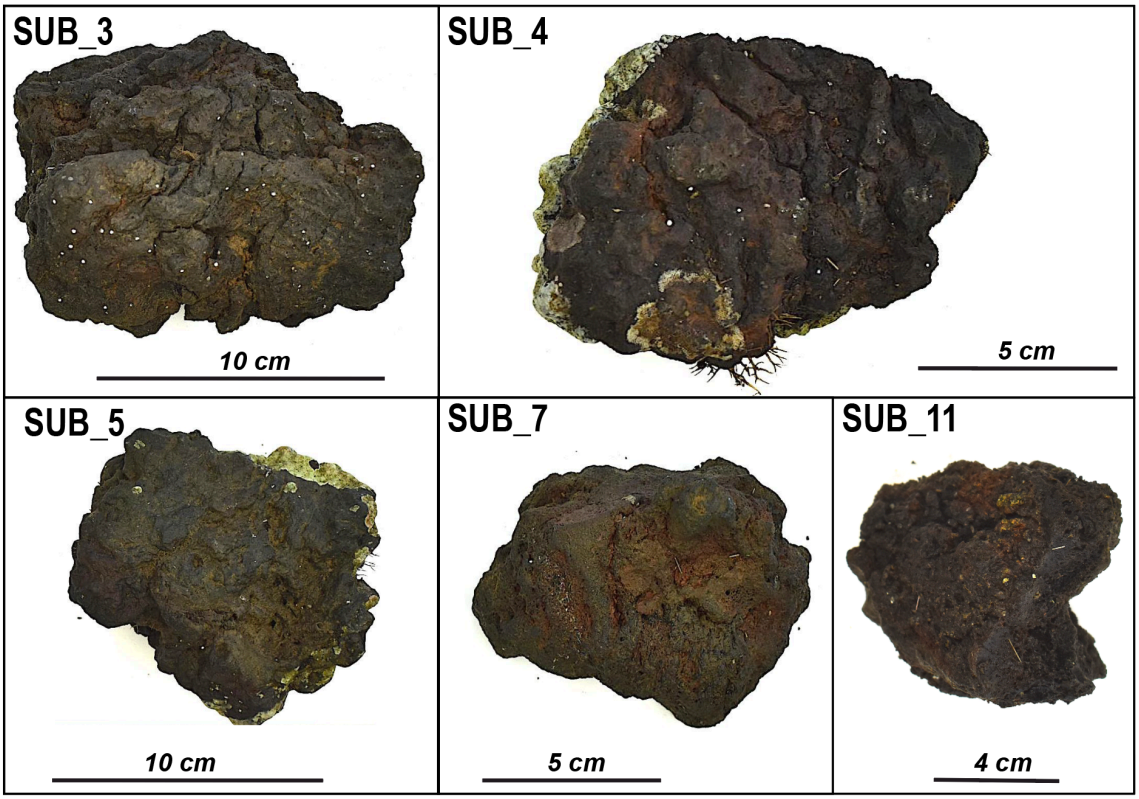

Figure S4. Examples of the largest hand-specimens collected by the divers at Stanley Patch volcano.

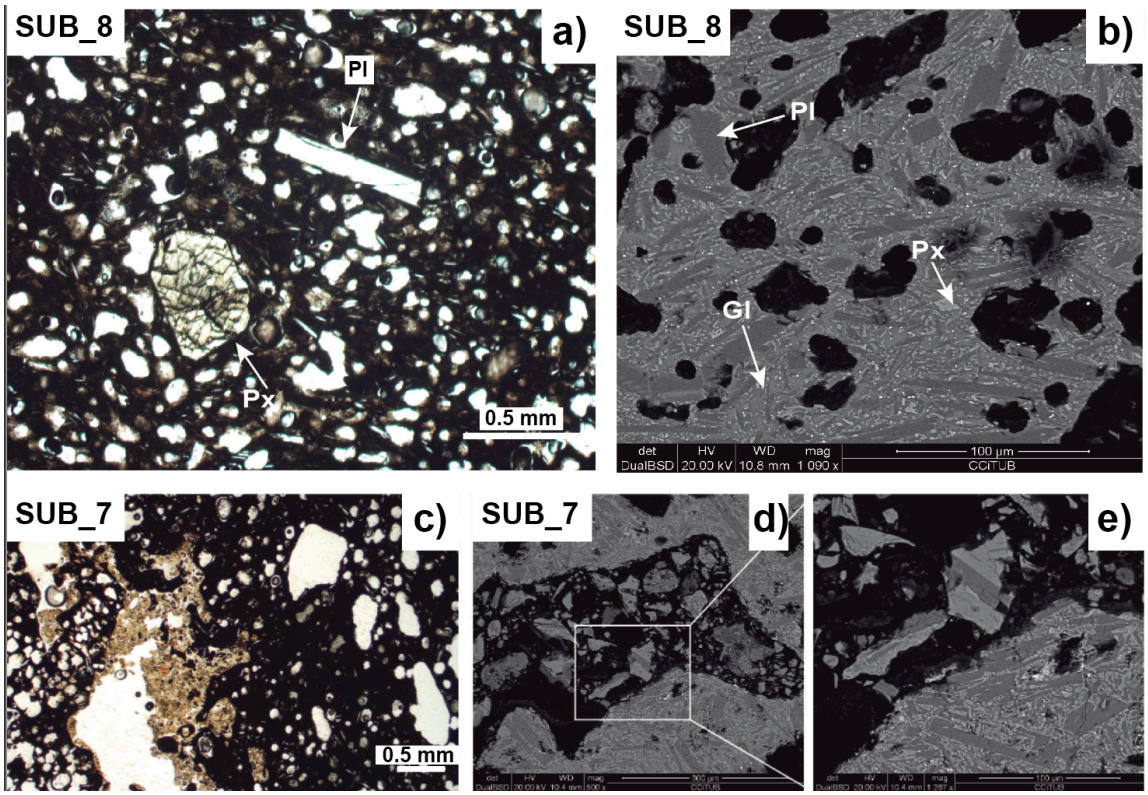

Figure S5. Plane light (a, and c) and SEM (b, d, and e) images of Stanley Patch juvenile samples. SUB_8 consists of a highly vesiculated scoriaceous volcanic fragment with phenocrysts of plagioclase (Pl) and pyroxene (Px) and with interstitial glass (GL). Images of sideromelane fragments filling vesicles in sample SUB_7 (c and d) and b) correspond to a porphyritic sample with plagioclase phenocrysts immersed in a dark crystalline groundmass of plagioclase (Pl), pyroxene (Px), oxides (Ox), and vesicles (Vs).

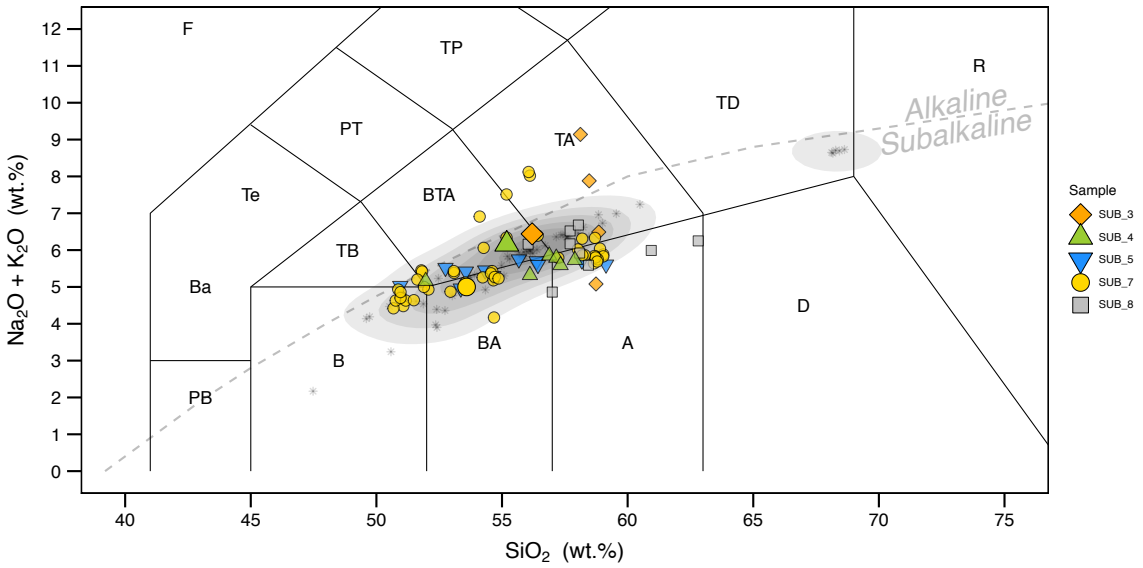

Figure S6. Total Alkali vs. Silica diagram (TAS) (Le Bas et al., 1986) for the rock samples considered in this work (see Table S3 for details on composition and exact latitude-longitude coordinates of the rock samples). For comparison grey shaded areas and asterisks correspond to the post-caldera rock samples presented by Geyer et al. (2019). Major elements normalized to 100% (anhydrous) with Fe distributed between FeO and Fe_2O_3 following Middlemost (1989). Grey dashed line discriminates between the alkaline-subalkaline fields (Irvine & Baragar, 1971). Analysis was conducted in R (R Core Team, 2014) and figure was produced using the package ggplot2 (Wickham, 2009).

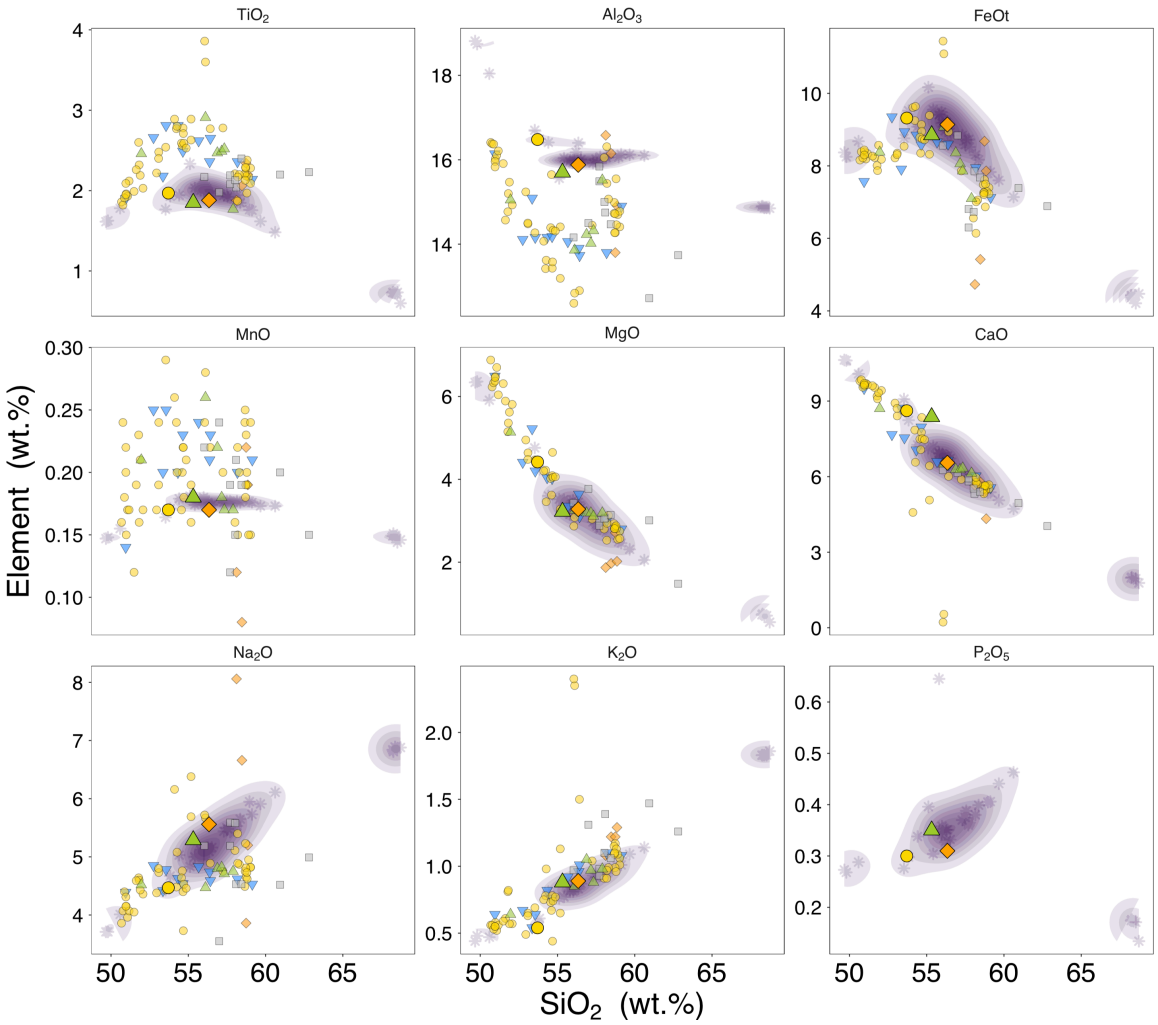

Figure S7. Major elements vs. SiO_2 content Harker Diagrams for the rock samples considered in this work. (See Table S3 for details on composition and exact latitude-longitude coordinates of the rock samples). For comparison grey-purple shaded areas and asterisks correspond to the post-caldera rock samples presented by Geyer et al. (2019). Major element compositions have been normalized to 100% in an anhydrous base with Fe as FeOt. Legend as per Figure S6. Analysis was conducted in R (R Core Team, 2014) and figure was produced using the package ggplot2 (Wickham, 2009).

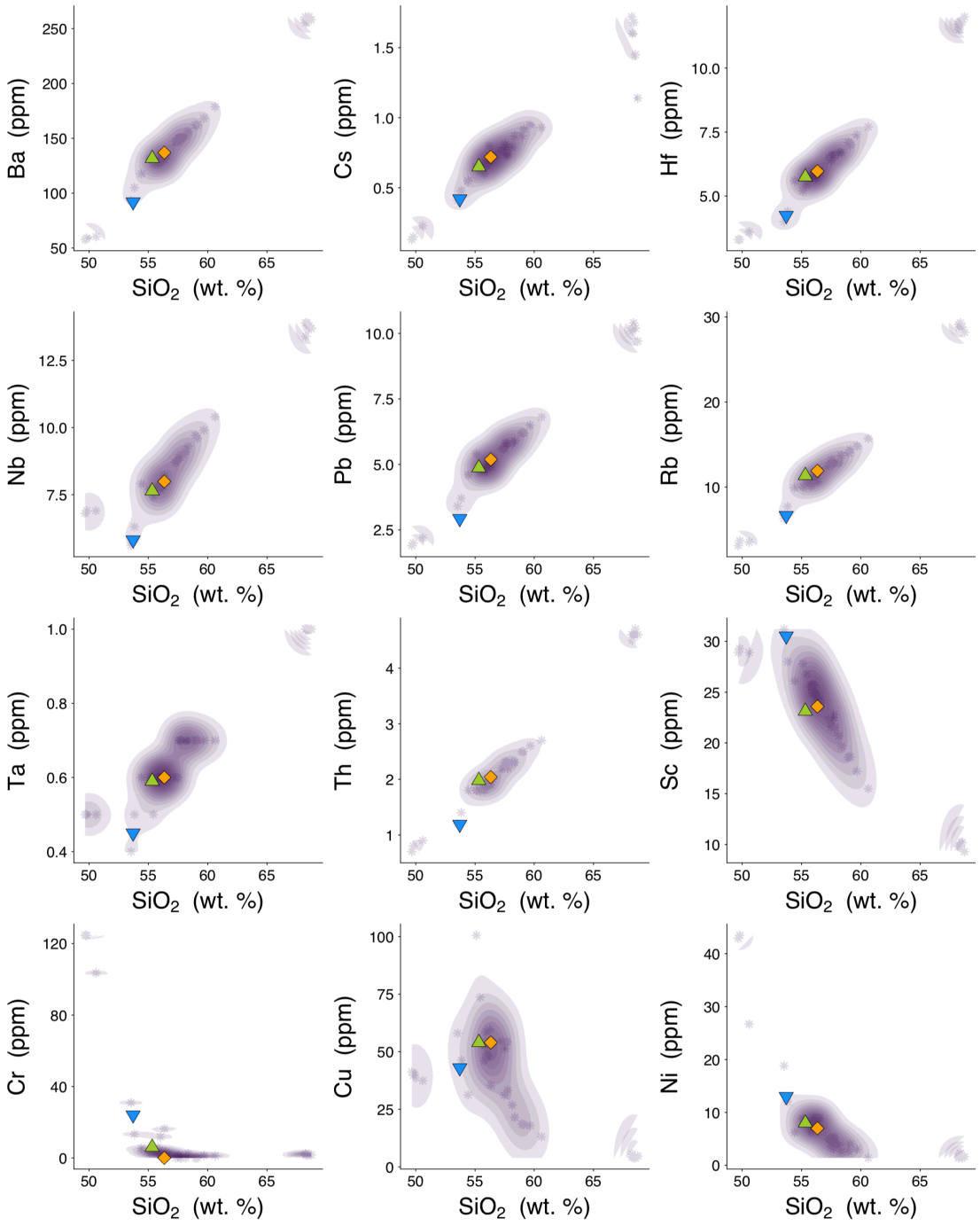

Figure S8. Trace and Rare Earth elements vs. SiO_2 content Harker Diagrams for the rock samples considered in this work. (See Table S3 for details on composition and exact latitude-longitude coordinates of the rock samples). For comparison grey-purple shaded areas and asterisks correspond to the post-caldera rock samples presented by Geyer et al. (2019). Major element compositions have been normalized to 100% in an anhydrous base with Fe as FeOt. Legend as per Figure S6. Analysis was conducted in R (R Core Team, 2014) and figure was produced using the package ggplot2 (Wickham, 2009).

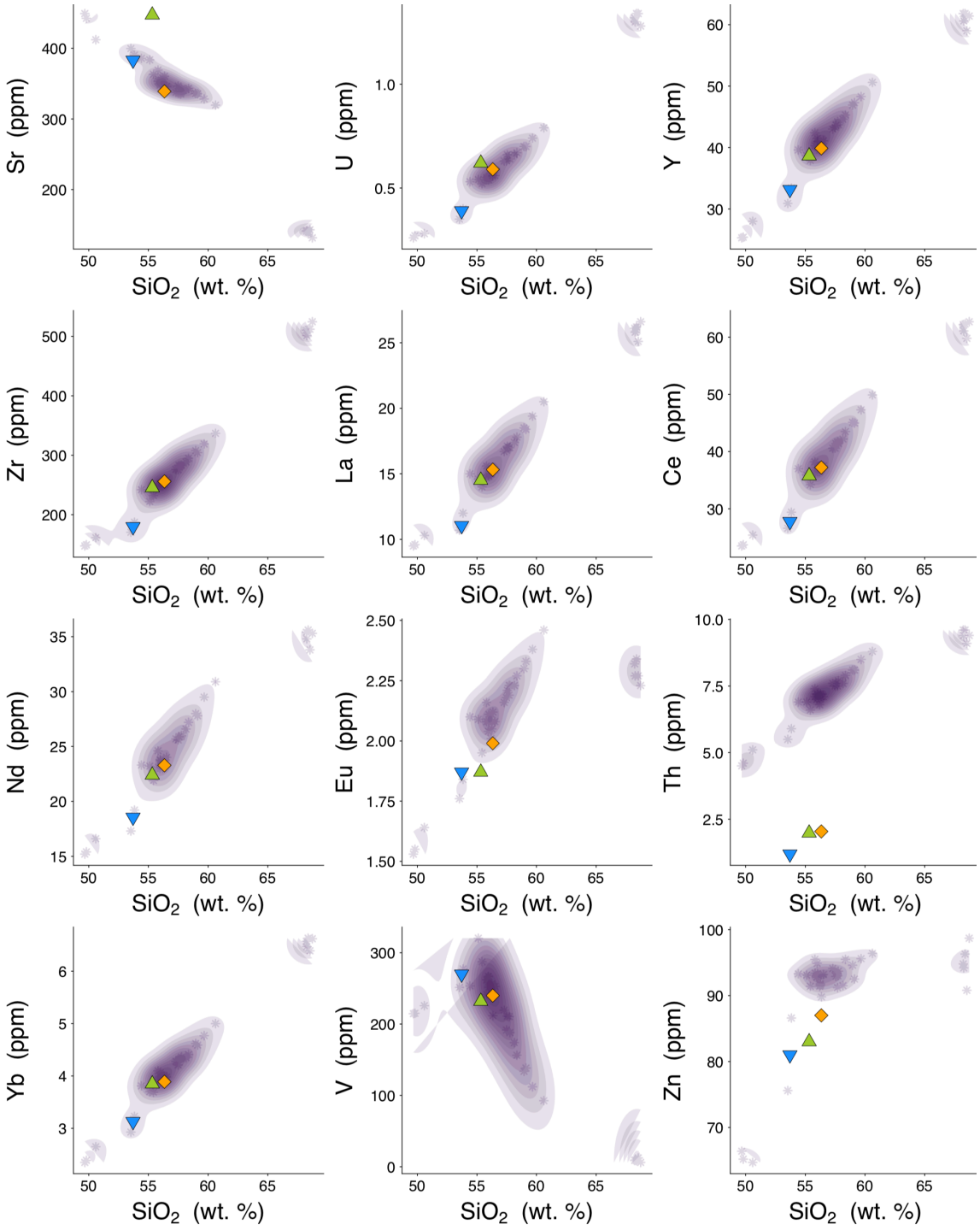

Figure S8. Continuation.

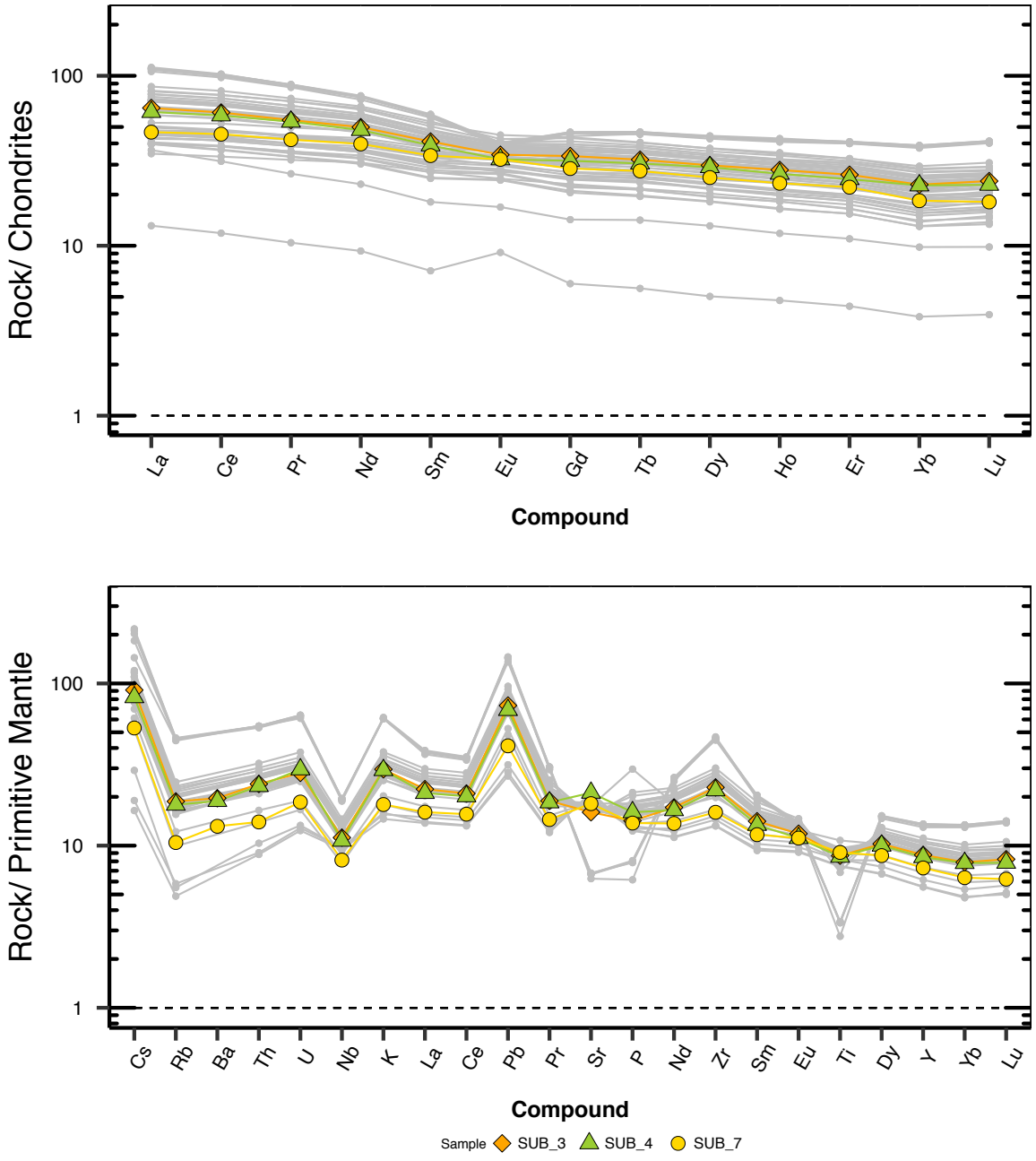

Figure S9. Whole Rock compositions normalized to chondrites (top) and primitive mantle (bottom) compositions of Sun and McDonough (1989). Major element compositions have been normalized to 100% in an anhydrous base with Fe as FeOt. Analysis was conducted in R (R Core Team, 2014) and figure was produced using the package ggplot2 (Wickham, 2009).

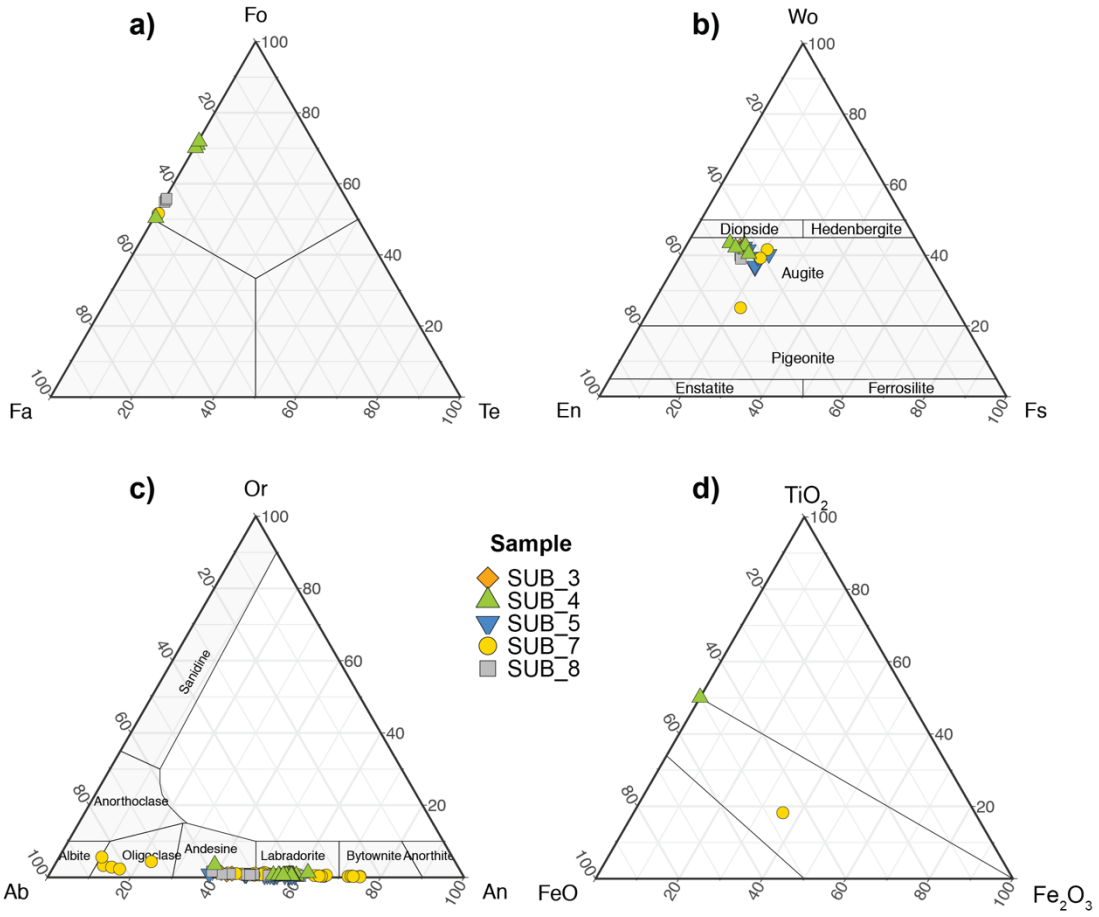

Figure S10. a) Forsterite (Fo) - Fayalite (Fa) - Tephroite (Te) ternary diagram for olivine classification; b) Wollastonite (Wo) - Enstatite (En) - Ferrosilite (Fs) ternary diagram for the classification of Ca-Mg-Fe pyroxenes (Morimoto, 1960); c) Orthoclase (Or) - Albite (Ab) - Anorthite (An) ternary diagram for the classification of feldspars (Deer et al., 2001); d) Ternary classification diagram for Fe-Ti oxides (Chang et al., 1998) (see Tables S5 to S8 for details on composition and exact latitude-longitude coordinates of the rock samples). Analysis was conducted in R (R Core Team, 2014) and ternary diagrams were developed with ggtern package for R (Hamilton and Ferry, 2018).

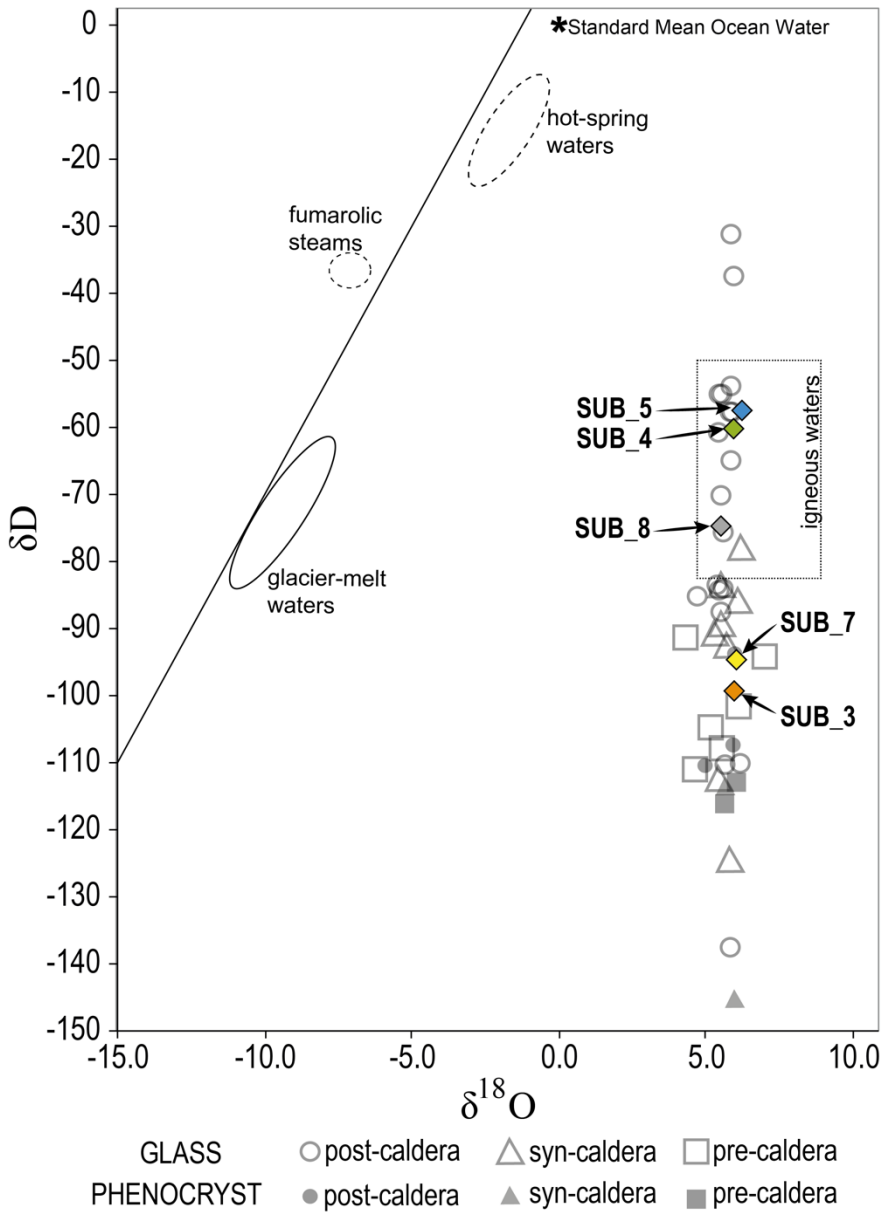

Figure S11. Plot of D vs O stable isotopes for the Stanley Patch samples. Deception Island samples are also represented according to their stratigraphic position (pre-, syn-, and post-caldera). Hot-spring, fumarolic, and glacier-melt waters data (ellipses) correspond to the local values at Deception Island from Kusakabe et al. (2009).

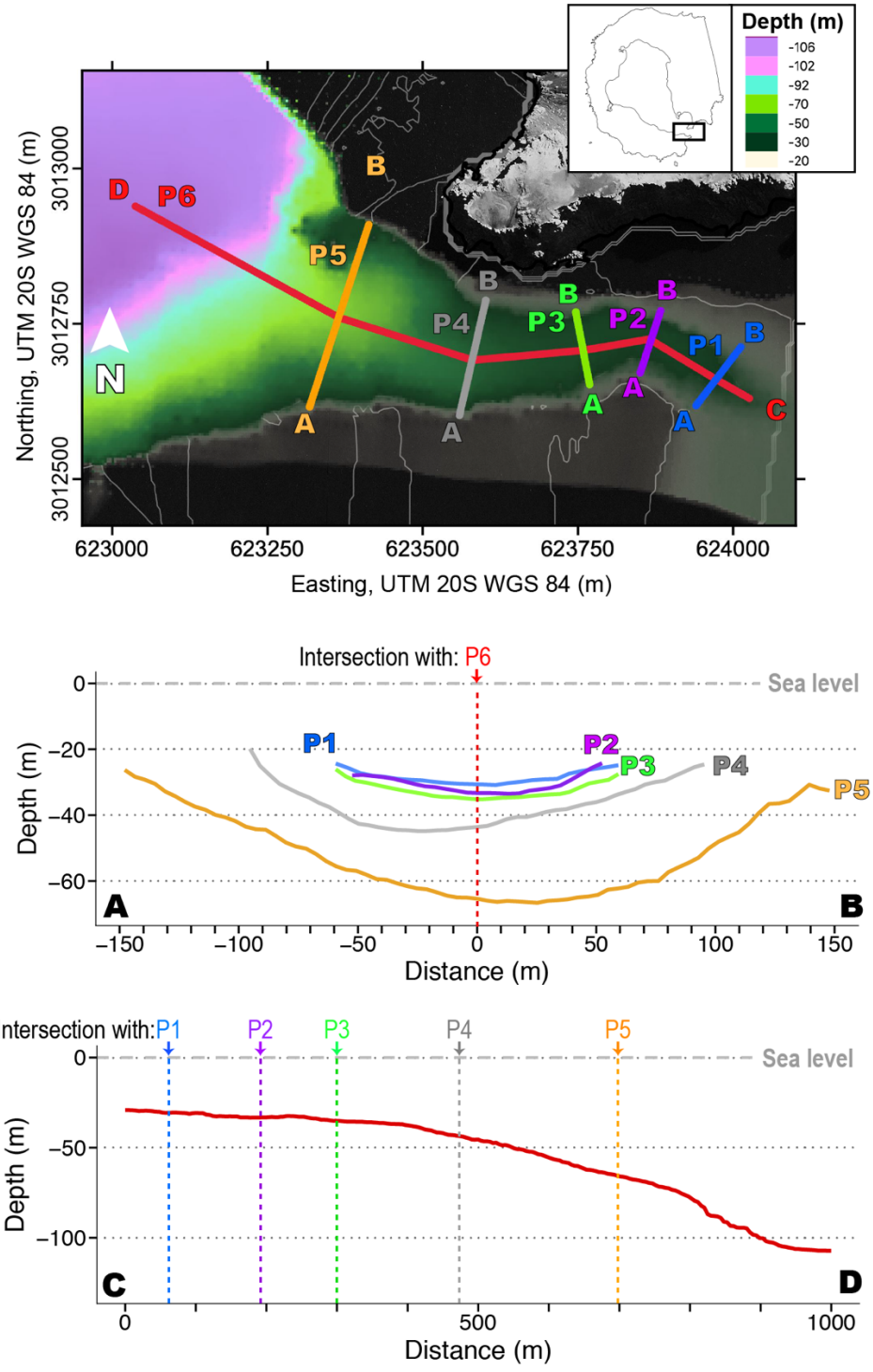

Figure S12. Bathymetric profiles across (P1 to P5) and along (P6) Neptunes Bellows.

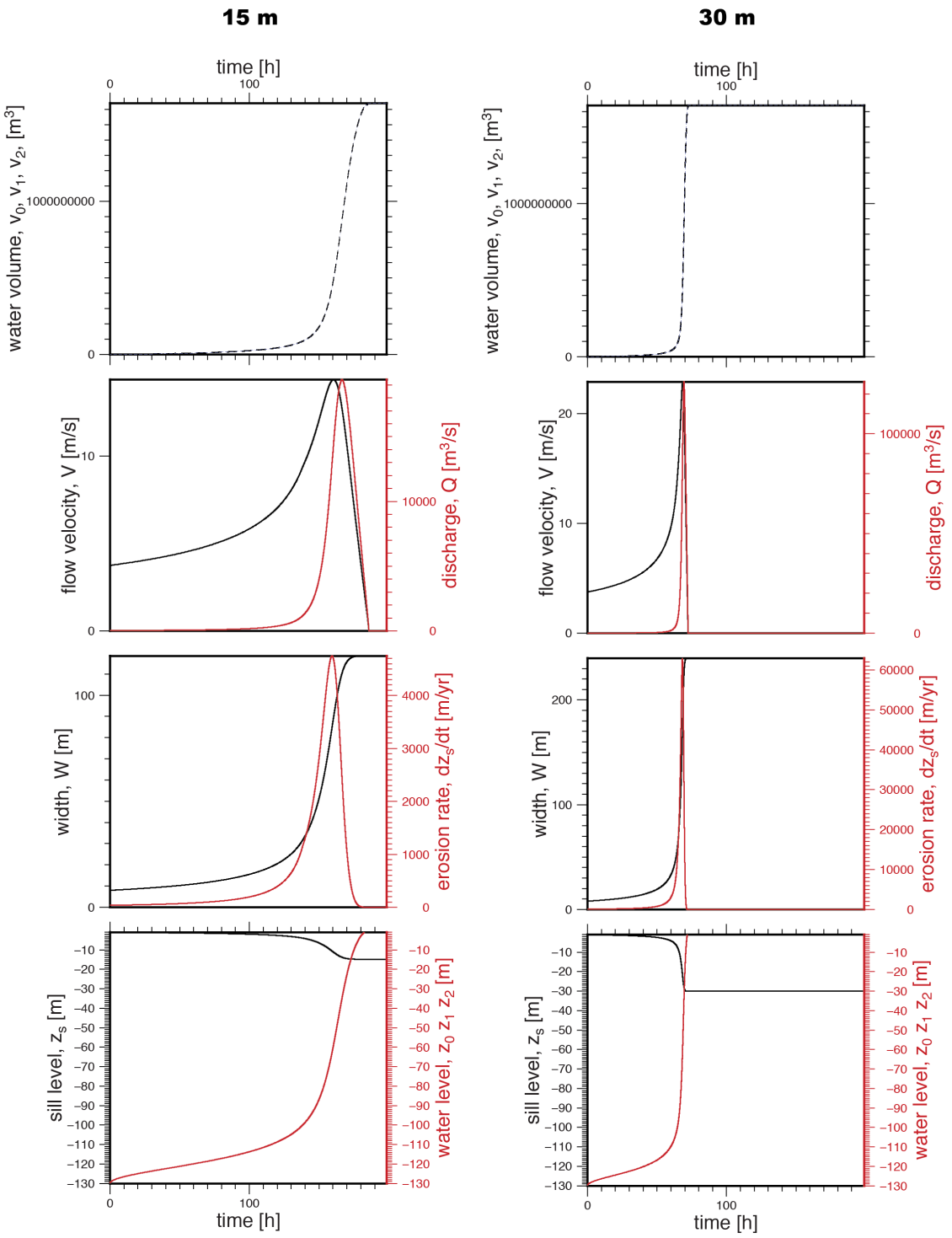

Figure S13. Numerical model results of flood development after breaching or overtopping for two final sill depths: 15m (left) and 30 m (right).

Table S1. Acquisition and processing parameters configuration applied during the Galileo-IHM 2018 Cruise.

ACQUISITION AND CONFIGURATION PARAMETERS							
ACQUISITION			**PROCESSING**				
TRANSMITTER	Transmitter Mode	Normal	FILTERS	Filter	Active		
	Trigger Mode	Internal		Filter Type	Matched		
	Trig Interval	Manual		Corner Frequency	Auto		
	Ping Interval [ms]	1500		Replica Shaped	Active		
	Pulse Form	Chirp (LFM)	TVG				
	Start Frequency [kHz]	2		TVG	Active		
	Stop Frequency [kHz]	5.5		TVG Control	Tracking		
	Chirp Lenght [ms]	10		Offset [ms]	-50		
	Output Level [dB]	0					
	Output Level [%]	100					
	HRP Stabilization	Active			**Length [ms]**	**Slope [dB/ms]**	
	Beam Control	Auto		Section A-B	5.4	0.78	
	Transducer Sound Speec	1510		Section B-C	25.9	0.77	
RECEIVER 1	Delay Control	Manual/Auto		Section C-D	35.6	0.14	
	Master Trig Delay [ms]	Variable With Depth					
	Delay Offset [ms]	30	GAIN	Gain	Active		
	Sample Rate [kHz]	16		Auto Gain [dB]	7.5		
	Trace Rate [kHz]	400		Filter Coefficient	0		
	Gain [dB]	22-34		Mute	Active		
	HP-Filter [kHz]	2		Mute [ms]	10		